Identification of Glyoxalase A in Group B *Streptococcus* and its contribution to methylglyoxal tolerance and virulence

Madeline S. Akbari[1], Luke R. Joyce[1], Brady L. Spencer[1], Kevin S. McIver[2], and Kelly S. Doran[1#]

[1]Department of Immunology and Microbiology, School of Medicine, University of Colorado Anschutz Medical Campus, Aurora, Colorado USA

[2]Cell Biology and Molecular Genetics, Maryland Pathogen Research Institute, University of Maryland, College Park, Maryland, USA

#Corresponding author

Kelly S. Doran: kelly.doran@cuanschutz.edu, 303-724-3539

12800 E. 19th Ave, RC1-N, MS 8333, Aurora, Colorado, USA, 80045.

Key words: Group B Streptococcus, *Streptococcus agalactiae*, host-pathogen interactions, glycolysis, glyoxalase, methylglyoxal, bacteremia, neutrophils

Abstract (238)

Group B *Streptococcus* (GBS) is a Gram-positive pathobiont that commonly colonizes the gastrointestinal and lower female genital tracts but can cause sepsis and pneumonia in newborns and is a leading cause of neonatal meningitis. Despite the resulting disease severity, the pathogenesis of GBS is not completely understood, especially during the early phases of infection. To investigate GBS factors necessary for blood stream survival, we performed a transposon (Tn) mutant screen in our bacteremia infection model using a GBS *mariner* transposon mutant library previously developed by our group. We identified significantly underrepresented mutations in 628 genes that contribute to survival in the blood, including those encoding known virulence factors such as capsule, the β-hemolysin, and inorganic metal ion transport systems. Most of the underrepresented genes have not been previously characterized or studied in GBS, including *gloA* and *gloB,* which are homologs for genes involved in methylglyoxal (MG) detoxification. MG is a byproduct of glycolysis and a highly reactive toxic aldehyde that is elevated in immune cells during infection. Here, we observed MG sensitivity across multiple GBS isolates and confirm that *gloA* contributes to MG tolerance and invasive GBS infection. We show specifically that *gloA* contributes to GBS survival in the presence of neutrophils and depleting neutrophils in mice abrogates the decreased survival and infection of the *gloA* mutant. The requirement of the glyoxalase pathway during GBS infection suggests that MG detoxification is important for bacterial survival during host-pathogen interactions.

Importance (146)

A transposon-mutant screen of group B *Streptococcus* (GBS) in a bacteremia mouse model of infection revealed virulence factors known to be important for GBS survival such as the capsule, β-hemolysin/cytolysin, and genes involved in metal homeostasis. Many uncharacterized factors were also identified including genes that are part of the metabolic pathway that breaks down methylglyoxal (MG). The glyoxalase pathway is the most ubiquitous metabolic pathway for MG breakdown and is only a two-step process using glyoxalase A (*gloA*) and B (*gloB*) enzymes. MG is a highly reactive byproduct of glycolysis and is made my most cells. Here, we show that in GBS, the first enzyme in the glyoxalase pathway, encoded by *gloA*, contributes to MG resistance and blood survival. We further demonstrate that GloA contributes to GBS survival against neutrophils *in vitro* and *in vivo* and, therefore, is an important virulence factor required for invasive infection.

Introduction

Streptococcus agalactiae (group B *Streptococcus*, GBS) is an opportunistic pathogen that commonly resides in the gastrointestinal and lower female genital tracts but can cause infection in newborns and is also increasingly associated with non-pregnant individuals, especially older adults and patients with diabetes (*1-3*). GBS asymptomatically colonizes the vaginal tract in up to 30% of people but can instigate complications during pregnancy and birth, such as preterm labor, and serious infections in newborns, such as sepsis, pneumonia, and meningitis (*1, 4-6*). Research into GBS intrauterine infection during pregnancy thus far indicates that GBS-activated inflammatory pathways ultimately result in preterm births (*7*). If GBS is vertically transferred to the neonate, the resulting infection is categorized as either early-onset disease (EOD, 0-6 days of life) or late-onset disease (LOD, 7-90 days of life) depending on the timing of symptom

presentation (*8*). Neonatal meningitis caused by GBS requires a sustained level of bacteremia prior to the penetration into the brain and, even after treatment, frequently results in long-lasting neurological effects and long-term morbidity (*4, 5*). Although intrapartum antibiotic prophylaxis (IAP) is administered to colonized pregnant women to prevent the detrimental effects of GBS infection, GBS isolates are increasing in resistance to second-line antibiotics over time (*9*) and IAP is not effective in preventing LOD. Therefore, studying GBS pathogenesis of meningitis, including bacteremia, is important for the development of novel treatments and therapeutics to prevent GBS infection and reduce morbidity and mortality.

Previous work has determined the GBS transcriptome as well as genes necessary for survival in human blood *in vitro* and for colonization and survival of the murine female reproductive tract (FRT) (*10-13*). These datasets as well as other studies have shown that GBS possesses an arsenal of virulence factors that directly contribute to pathogenesis such as β-hemolysin/cytolysin, superoxide dismutase, capsule, adherence proteins, and metal transport systems (*10, 14, 15*). β-hemolysin/cytolysin (βH/C) and capsular polysaccharide (PS) are the most well studied factors associated with GBS pathogenesis and are regulated by the well-known two-component system, CovR/S (*15*). βH/C is an ornithine rhamnolipid pigment synthesized by the *cyl* operon and has both hemolytic and cytolytic capabilities against a variety of host cells including red blood cells, neutrophils, macrophages, and epithelial cells (*16-19*). As a result, βH/C has been shown to contribute to GBS blood, lung, and brain infection (*17, 20*). Capsular PS is surface-associated and made up of different arrangements of monosaccharides that form capsular repeat units (*21, 22*). There are 10 known GBS capsular serotypes with serotype III the main serotype associated with neonatal infections, like meningitis, since it is overrepresented in isolates worldwide (*9, 23, 24*). Group B streptococcal capsular PS was first studied over 40 years

ago and has been shown to help GBS evade host immune defenses by mimicking host antigens and blocking complement-mediated opsonophagocytic killing as well as to facilitate GBS biofilm formation (*22, 25-27*). Despite these studies into a few important virulence factors, the contribution of GBS metabolism to colonization and infection *in vivo* has been a neglected area of study in the field (*10, 15*).

Here we performed a transposon-mutant screen (Tn-sequencing) using a murine bacteremia model to discover additional genes necessary for GBS fitness in murine blood *in vivo*. GBS survival within the blood is an essential prerequisite to penetrate the blood brain barrier and subsequence development of meningitis. Tn-sequencing allows us to capture genes that may be continuously expressed but are essential in certain environments. Here, we identify that the glyoxalase pathway is required for GBS bloodstream survival. The glyoxalase pathway consists of two genes, *gloA* and *gloB,* and is involved in methylglyoxal detoxification. Methylglyoxal (MG) is toxic byproduct of normal cell metabolism, and we confirm that the first enzyme in the pathway, encoded by *gloA*, contributes to GBS MG detoxification and invasive infection. Furthermore, we found that *gloA* is necessary for GBS survival against neutrophils and that neutrophils contribute to decreased *gloA* mutant virulence *in vivo*.

Results

Genome-wide analysis of GBS factors involved in bloodstream survival.

To identify genes necessary for GBS survival in murine blood, we utilized a bacteremia model of infection with our previously described Tn mutant library in the CJB111 strain (*17, 28-30*). Briefly, mice were intravenously infected with the Tn mutant library and the infection was allowed to progress up to 27 hours. The input Tn mutant library and libraries recovered from the

blood were processed as described in Materials and Methods. To identify transposon insertion sites, sequenced reads were mapped to the GBS CJB111 genome, which identified 628 genes as significantly underrepresented and 95 genes as significantly overrepresented in the blood compared to the input library (**Fig. 1A**) (**Table S1**). The significant gene hits were equally distributed across the genome. Significant genes were then assigned clusters of orthologous groups of proteins (COGs). The number of significant gene hits in each COG were normalized to the total number of genes in each COG revealing sRNA, amino acid transport and metabolism, and inorganic ion transport and metabolism as the COGs containing the most underrepresented genes during GBS survival in the blood (**Fig. 1B**). We detected many classes of GBS virulence factors and genes known to contribute to GBS infection as significantly underrepresented (**Table 1).** Some of these genes are involved in hemolytic pigment biosynthesis, capsule biosynthesis, two-component regulatory systems, metal transport, glutamine transport, and purine metabolism. When we investigated other underrepresented genes that have not been previously characterized in GBS, we found homologous genes to glyoxalase A and B of the glyoxalase pathway to both be significantly underrepresented with fold changes of -18.38 and -25.63, respectively (**Table 1**). The glyoxalase pathway is a ubiquitous two-step process found across all kingdoms of life and is the primary mechanism of methylglyoxal (MG) breakdown (**Fig. 1C**) (*31*). A highly reactive carbonyl byproduct of normal cell metabolism, most MG is primarily generated from glycolysis, but can also be produced from other metabolic pathways such as lipid and protein metabolism (*32*).

Methylglyoxal tolerance differs across GBS strains.

GBS contains glyoxalase A and B homologs, also known as lactoylglutathione lyase and hydroxyacylglutathione hydrolase respectively. These are hypothesized to be involved in MG detoxification and therefore, tolerance. To begin to characterize this pathway in GBS, we grew several clinical GBS isolates in the presence of MG in a modified chemically defined media (mCDM) (*62*). Interestingly, different GBS isolates had varying degrees of resistance to MG with A909, H36B, CJB111, and 10/84 exhibiting the highest sensitivity and 2603 V/R exhibiting the most resistance to MG (**Fig. 2**). Isolate resistance did not correlate with serotype except for serotype III, which had the highest median %Growth at 35.8% compared to 18.8% (Ia), 8.1% (Ib), and 8.0% (V). To explore this difference in MG tolerance further, we selected three representative strains with low to high resistance: CJB111, A909, and COH1. First, we compared GloA amino acid sequences between these three strains and previously characterized GloA from *Streptococcus pyogenes*, *Listeria monocytogenes*, and *Escherichia coli* (**Fig. 3A**) (*63-66*). The GloA from CJB111 and A909 are 100% identical while the COH1 GloA is 99% identical due to a single amino acid change of an alanine to a serine (A45S) in a non-conserved region. To determine how common this variant was in GBS, we generated a phylogenetic tree using BlastP and FigTree to compare 57 GBS genomes and found 12 out of 57 GloA proteins (21%) have the A45S change with another 5 having a different A45 variant (**Fig. 3B**). Proteins with the A45S variant also clustered together in the tree suggesting a common ancestral strain. To assess tertiary structure, a predicted protein model for GBS GloA was generated using AlphaFold2 that had extremely high confidence for most residues (**Fig. 3C & S1**). The predicted structure was compared to the solved *E. coli* GloA structure (PDB 19FZ) and found to have highly similar topology and conserved metal binding residues (**Fig. 3C**). GloA was also modeled in its active form as a dimer to show predicted active sites (**Fig. 3D**). The A45S variant from COH1 GloA

was included in the dimer and modeled to be next to the predicted active site. Lastly, using our selected representative strains, we investigated baseline transcription regulation of the glyoxalase pathway by comparing mid-log transcript levels for *gloA* and *gloB* using RT-qPCR, and found that COH1 has higher abundance of both *gloA* and *gloB* transcripts compared to CJB111 and A909 (**Fig. S2**).

Glyoxalase A contributes to methylglyoxal detoxification in GBS.

To confirm our Tn-sequencing results we chose to study the first enzyme in the glyoxalase pathway, GloA. Using allelic exchange mutagenesis, we constructed a mutant in *gloA* (Δ*gloA*) and a complemented strain (p*gloA*) in CJB111 as described in Materials and Methods. MG detoxification was then tested using these strains by MG quantification and growth curve analysis. First, to measure if MG accumulates in the Δ*gloA* strain, we measured MG concentrations using ELISA on lysed cell pellet samples for CJB111 WT, Δ*gloA*, and p*gloA* strains. The concentration of MG was normalized to the total protein concentration of each sample and found to be significantly increased in the Δ*gloA* mutant compared to the CJB111 WT and complemented strains (**Fig. 4A**). To determine if this accumulated MG in the gloA mutant may be toxic/impact GBS growth, next, all strains were inoculated into mCDM with or without the addition of 0.5 mM MG. Indeed, a growth delay was observed for Δ*gloA* with the addition of MG (**Fig. 4B**). OD_{600} at 8 hrs was compared between strains and confirmed a significant decrease in Δ*gloA* growth compared to WT or the complemented strain following the addition of MG (**Fig. 4C**). As MG is primarily produced from glycolysis in cells, we further investigated the impact of GloA on GBS growth in mCDM with increasing glucose concentrations. However, we did not observe a growth defect for the Δ*gloA* mutant compared to WT or complemented strain at

any glucose concentrations tested (**Fig. S3A**). Additionally, upon assessment of general virulence characteristics, we also did not observe a difference in susceptibility to hydrogen peroxide or hemolytic activity between CJB111, Δ*gloA*, and p*gloA* (**Fig. S3 B,C**). Taken together MG quantification and growth analysis suggest that GloA contributes to MG detoxification in GBS. Our results also suggest that under these conditions tested, GBS does not produce enough MG from glucose metabolism to negatively impact its growth.

Glyoxalase A is necessary for GBS survival *in vivo*.

To further confirm the Tn-sequencing results and determine if *gloA* is important during infection, we repeated our bacteremia model of infection by intravenously injecting mice with 1.5-2 x 10^7 CFU CJB111 WT or the Δ*gloA* mutant and monitoring the infection for up to 72 hours post-infection. Mice infected with the Δ*gloA* mutant exhibited significantly decreased mortality compared to those infected with WT, with greater than 75% surviving to the experiment endpoint (**Fig. 5A**). In order to monitor CFU burden over-time, blood samples were taken from surviving mice at 24 and 48 hrs post-infection and at time-of-death (TOD). Mice infected with Δ*gloA* had significantly decreased blood burdens at all time-points and in tissues at the time of death, indicating the mutant strain is not able to survive as well in the bloodstream and disseminate to other organs compared to WT CJB111 (**Fig. 5B-C**).

Importance of GBS Glyoxalase A to Neutrophil Survival

Neutrophils are the primary immune cell GBS encounters during acute infection (*53*), and have been shown to produce aldehydes, such as MG in response to infection (*64, 67-69*). To determine if GBS *gloA* contributes to neutrophil survival we performed *in vitro* neutrophil killing assays

using differentiated HL60 neutrophil-like cells with the CJB111 WT, Δ*gloA*, and p*gloA* strains. At 5 hrs post-infection, the Δ*gloA* mutant strain exhibited significantly decreased survival compared to WT or the complemented strains (**Fig. 6A**). This phenotype was independent of serum killing since serum by itself did not impact GBS survival over time (**Fig. S4A**). To evaluate if this increased killing might be due to increased HL60 production of MG in response to GBS infection, we measured the accumulation of intracellular MG-modified proteins using flow cytometry. Consistent with the literature (*70*) we observed that all cells contained detectable MG-modified proteins. Interestingly, however, upon infection, we observed a two-fold increase in anti-MG mean fluorescent intensity (MFI) compared to uninfected controls (**Fig. 6B**), indicating that infection increases intracellular MG within HL60s. This increase was also only observed in high glucose conditions (**Fig. S4B**), which is similar to what has been described for *S. pyogenes* where they observed that GloA contributed to neutrophil survival under high glucose concentrations (*63*). To examine the contribution of neutrophils to control of GBS infection *in vivo,* we depleted neutrophils in mice prior to intravenous infection. Mice were injected intraperitoneally with anti-Ly6G or an isotype control 24 hrs (*71*) before intravenous infection with 1 x 10^7 CFU CJB111 or Δ*gloA*. At 12 hours post-infection, we observed that neutrophil depletion abrogated the attenuated phenotype of the Δ*gloA* mutant in the blood, as the CJB111 and Δ*gloA*-infected, neutrophil depleted mice did not differ in blood burdens. Further, CJB111 and Δ*gloA* CFU burdens were significantly increased in the neutrophil-depleted mice compared to the non-depleted mice (**Fig. 6D).** Upon assessing morbidity and mortality of these groups over 72 hours post-infection, we observed that both the CJB111 and Δ*gloA*-infected, neutrophil depleted mice exhibited significant increases in mortality when compared to their non-depleted cohorts (**Fig. 6C**), although percent survival of neutrophil-depleted mice infected with Δ*gloA*

remained higher than neutrophil-depleted mice infected with CJB111. Taken together these results show that the mutant phenotype can be partially rescued with neutrophil depletion and suggest that MG produced by other cell types may aid in the defense against GBS bloodstream infections.

Discussion

GBS must be able to survive multiple host niches to cause invasive infection in neonates. Some of these environments include the vaginal tract, amniotic fluid, and blood (*1, 72*). Tn-sequencing is a powerful and common method for investigating bacterial genes necessary for survival and fitness in these different environments. Previously, an *ex vivo* Tn-sequencing was performed in human blood by Hooven *et al.* 2017 using a TnSeq library in the GBS A909 serotype Ia background (*73*). Their results found similar underrepresented genes compared to our *in vivo* dataset such as genes involved in capsule biosynthesis, metal homeostasis, and arginine metabolism. Interestingly, they identified *relA* to be underrepresented, which encodes a GTP pyrophosphokinase and is a central regulator of the stringent response in GBS. They found that *relA* not only controls stringent response activation and the arginine deiminase pathway but also impacts βH/C production. While we did not observe *relA* in our dataset, other putative stress response proteins like *ytgB* and *asp1* were significantly underrepresented. Most notably, *asp1* is annotated as an Asp[23]/Gls[24] family envelope stress response protein and was found to be upregulated when GBS was incubated in human blood (*13, 74*) and downregulated after exposure to high glucose (*75*). We also observed that the two-component system (TCS) *dltRS* and a *dlt* gene were underrepresented, which are involved in modulating surface charge and contribute to cationic antimicrobial peptide resistance and decrease phagocytic killing (*33, 52*).

Previous studies have shown that a *dltA* mutant exhibited decreased virulence in a murine model with significantly lower burdens in tissue and blood compared to WT GBS (*33*). Another TCS, *bceRS/nsrRK,* exhibited the highest negative fold change of the underrepresented TCS and has been shown to contribute to bacitracin (antibiotic), nisin (lantibiotic), cathelicidin/LL-37 (human antimicrobial peptide), and oxidative stress resistance (*54, 55*). Its role in GBS pathogenesis was demonstrated as a *bceR* mutant yielded decreased virulence during murine infection and decreased biofilm formation (*54*). Another top gene hit identified within the present study to be important for GBS blood survival is the C5a peptidase *scpB. scpB* is already known to be involved in complement evasion and fibronectin binding and is associated with neonatal isolates (*34, 76*). Overall, identifying these known virulence factors in our study demonstrates the validity of our *in vivo* Tn-sequencing screen to identify novel factors important for blood survival in mice and supports previous research in the streptococcal field. It also provides another resource for developing new hypotheses and research projects. For example, methylglyoxal (MG) detoxification has not been previously characterized in prior GBS studies.

MG is a highly reactive electrophilic species (RES) and byproduct of normal cell metabolism which can be spontaneously or enzymatically produced by all cells (*31, 70*) with up to 90% of cell MG estimated to come from glycolysis alone (*77*). Notably, MG is also a precursor to advanced glycation end products (AGEs) and is associated with many other human diseases like diabetes, cancer, and neurological disorders like Alzheimer's disease (*70, 78*). The most well-known and ubiquitous pathway for MG detoxification is the glyoxalase pathway which consists of glyoxalase A (*gloA*) and glyoxalase B (*gloB*) enzymes. Recently, the glyoxalase pathway, especially *gloA,* in *L. monocytogenes* was found to contribute to intracellular survival in macrophages and during murine infection (*64*). In addition, the glyoxalase pathway in *S.*

pyogenes was shown to be important for survival against neutrophils in a glucose and myeloperoxidase dependent manor (*63*). The GBS *gloA* and *gloB* homologs were underrepresented in our Tn-sequencing dataset which suggested that GBS may encounter high levels of MG during bloodstream infection. Therefore, we hypothesized that GBS may encounter host-derived MG during bacteremia as a response to infection (*63, 67, 79, 80*). The first step in the glyoxalase pathway is mediated by GloA and, in this study, we have characterized its contribution to GBS MG tolerance *in vitro* and infection *in vivo*. We observed that a *gloA* mutant exhibited decreased survival in the presence of neutrophils and that this attenuation was largely abrogated in neutrophil-depleted mice. We also measured an increase in MG-modified proteins in neutrophil-like cells upon GBS infection which is likely from increased production of MG by the neutrophil-like cells themselves. These results indicate MG-mediated killing may constitute another important defense mechanism used by immune cells to kill invading bacteria.

Looking into MG detoxification in other GBS isolates, we observed that tolerance to MG varies and is not definitively correlated to GloA amino acid sequence or glyoxalase gene regulation. Of note, serotype III strains, the most commonly isolated serotype from neonatal invasive infections (*81*), appear to have the highest overall tolerance to MG, although additional strains would need to be tested to substantiate this observation. Interestingly, COH1 (serotype III) had high resistance to MG and was the only strain tested that had the A45S variant in GloA and higher baseline transcript levels of *gloA* and *gloB* compared to CJB111 and A909 strains. The A45S variant is also only 10 amino acids away from the K55 residue which is predicted to be involved in metal binding and could impact folding or metal coordination (*66, 82, 83*). However, other GBS strains tested also had high resistance to MG, like 515, which does not have the A45S variant. Therefore, it is unlikely that this amino acid change is the sole determinant of

enzyme activity, but further investigation is needed to determine if GloA protein variants and regulation impact GBS MG tolerance. Relatedly, *S. mutans* was shown to be more tolerant to MG than most other commensal oral Streptococcal species and was also shown to outcompete *S. sanguinis* when MG was present in a competition experiment (*84*). From this previous study and our work shown here, we hypothesize that differences in GBS MG tolerance could be influenced by the presence of other bacterial species during colonization and infection.

Components of metal transport systems were also significantly underrepresented in the Tn-sequencing dataset with top hits including the zinc import system *adcAAIIBC* and *lmb,* the manganese import system *mtsABC,* and the putative nickel import system *nikABCDE* (**Table 1**). These results suggest GBS requires trace metals to survive in the blood and it has already been shown previously that zinc and manganese transporters are important for maintaining GBS metal homeostasis and contribute to vaginal colonization and FRT ascension and blood survival (*13, 29, 74, 85*). In addition, both zinc and manganese import systems are important in combating nutritional immunity, or the sequestration of nutrients by the host, mediated by a neutrophil-produced metal-binding protein called calprotectin (*30, 44*). The nickel transporter, however, has not been as well characterized. In our previous study, we attempted to measure nickel concentrations in a *nikA* mutant, but it was under the limit of detection in our samples. However, we did observe lower levels of copper indicating the system could be transporting more than one metal (*45*). There are only 9 known enzymes present in archaea, bacteria, plants, and primitive eukaryotes that are nickel dependent, with urease being the most notorious, but GBS does not encode a urease enzyme (*29, 45, 86, 87*). Interestingly, another of the 9 known enzymes is GloA which was found to use nickel (Ni^{2+}) as a cofactor in *E. coli* (*32, 66, 83*). Therefore, the

importance of the nickel transporter in the blood could be due to increased GloA activity. Overall, the requirement for nickel in GBS still remains to be elucidated.

MG is formed primarily from glycolysis but it can be produced, albeit to a lesser extent, from lipid, ketone, and protein metabolism (*32, 70*). MG is toxic to cells due to its electrophilic properties allowing it to react with different molecules, like DNA and protein, and affectively arrest growth (*79*). For example, MG has been shown to increase mutation rates in *L. monocytogenes* by binding DNA (*64*) and inhibits protein synthesis and modification by binding to guanine and arginine residues (*88-91*). It is important to note that in some bacteria, like *E. coli* and *L. monocytogenes,* MG can be formed directly from dihydroxyacetone phosphate (DHAP) during glycolysis by methylglyoxal synthase (*mgsA*); however, GBS, like other streptococci, do not have a MG synthase gene (*63, 84*). The lack of a synthase gene further supports our hypothesis that GBS encounters host-derived MG toxicity during infection. Since about 99% of cellular MG is thought to be already bound to molecules like DNA and protein it is difficult to quantify accurately; however, intracellular MG concentrations are consistently estimated below 10 µM and are known to be dependent on glutathione concentrations (*70, 92, 93*). In serum of diabetic individuals, the concentration of MG and MG-derived AGEs are increased compared to healthy individuals most likely due to increased glucose concentrations (*93*). MG is historically tied to diabetes because it is known to exacerbate diabetic complications like microvascular and kidney dysfunction and contribute to the progression of the disease (*93*). Our lab has shown that GBS is a common colonizer of infected diabetic wounds (*94*) and we show here the production of MG-modified proteins by neutrophil-like cells is dependent on glucose and GBS infection (**Fig. 6B**, **Fig. S4B**). Therefore, research into the role of the GBS glyoxalase pathway in the context of diabetic wound infection is a current area of study.

Lastly, conversion of MG to D-lactate by the glyoxalase pathway was first described over 100 years ago and is the most ubiquitous and conserved process for MG detoxification across all kingdoms of life (*31*). MG detoxification has not been thoroughly studied in streptococci in the context of disease and has never been characterized in GBS. Thus far, studies focusing on *S. pyogenes*, *S. mutans*, and *S. sanguinis* have shown *gloA* to be the primary modulator of MG tolerance *in vitro* with *gloB* mutants having little effect (*63, 84*). This is in support of what was observed with *L. monocytogenes*, but not *Salmonella* where it was found that *gloB* was more important for *Salmonella* resistance to oxidative stress and killing by macrophages (*64, 95*). Here, we found *gloA* to be dispensable to GBS tolerance of H_2O_2 (**Fig. S3B**) but the contribution of *gloB* remains to be investigated. There are also other enzymes that can break down MG into acetol or lactaldehyde intermediates including aldose, aldehyde, and MG reductases. A putative aldo/keto reductase (*yvgN*) was significantly underrepresented in our data set (**Table 1**) but its contribution to GBS virulence requires further investigation (*32*).

In this study we demonstrate, for the first time, an essential role of the glyoxalase pathway to GBS MG resistance and overall pathogenicity during bacteremia. We investigated the role of GloA *in vitro* and *in vivo* and confirmed it is important for growth in the presence of MG, survival against neutrophils, and during invasive infection. Our study also provides further evidence in support of the aldehyde hypothesis in that MG detoxification is an important component for bacterial survival against neutrophil metabolic defenses; however, the role of the glyoxalase system to GBS survival in macrophages requires further investigation (*67*). Research aimed at understanding metabolic mechanisms used by bacteria to survive in the blood and RES toxicity will be important for the development of new treatment and therapies for infection and will expand our knowledge about host-pathogen interactions.

Materials and Methods

Bacterial strains, media, and growth conditions. See Table S2 for strains and primers used in this study. GBS strains were grown statically at 37°C in THB, unless otherwise stated. Streptococcal chemically defined medium (*62*) was modified by omitting L-cysteine and adding 22mM glucose, unless otherwise stated. *Escherichia coli* strains for cloning were grown in LB at 30°C or 37°C with rotation at 250 rpm. Kanamycin and erythromycin (Sigma-Aldrich, St. Louis, MO) were supplemented to media at 50 µg/mL and 500 µg/mL, respectively, for *E. coli*. Kanamycin, spectinomycin, and erythromycin (Sigma-Aldrich, St. Louis, MO) were supplemented to media at 500 µg/mL, 100 µg/mL, and 5 µg/mL, respectively, for streptococcal strains.

Routine molecular biology techniques. All PCR reactions utilized Phusion or Q5 polymerase (Thermo Fisher, Waltham, MA). PCR products and restriction digest products were purified using QIAquick PCR purification kit (Qiagen, Venlo, NL) per manufacturer protocols. Plasmids were extracted using QIAprep miniprep kit or plasmid midi kit (Qiagen, Venlo, NL) per manufacturer protocols. Restriction enzyme digests utilized XmaI, EcoR1, and BamH1 (New England Biolabs, Ipswich, MA) for 2 hours at 37°C in a thermocycler. Ligations utilized Quick ligase (New England Biolabs, Ipswich, MA) at room temperature for 5 min or Gibson Assembly Master Mix (New England Biolabs, Ipswich, MA) per manufacturer protocols. All plasmid constructs were sequence confirmed by Sanger sequencing (CU Anschutz Molecular Biology Core, Aurora, CO) or whole plasmid sequencing (Quantara Biosciences, Hayward, CA).

The mutant strains were generated as previously described (*12, 29*). Briefly, for the *gloA* mutant, genomic 5' and 3' regions flanking the *gloA* gene were amplified and fused with a spectinomycin cassette by FailSafe PCR (Lucigen, Middleton, WI). Fragments and pHY304 vector were digested with restriction enzymes and ligated using Quick Ligase. The ligation reaction product was transformed into chemically competent *E. coli*. pHY304 plasmids were purified from *E. coli* and electroporated into GBS CJB111 genetic background. Constructs were confirmed by PCR and sequencing. Complement strains were generated by amplifying the *gloA* gene in GBS and linearizing pABG5 by PCR. Products were ligated using Gibson assembly and then transformed into chemically competent *E. coli*. Plasmids were purified from *E. coli* and electroporated into GBS CJB111 Δ*gloA* genetic background. Primers used in the construction of strains are listed in Table S2. The mutant had no growth or hemolysis defects observed (**Fig. S3A&C**).

Study approval. Animal experiments were approved by the Institutional Animal Care and Use Committee (IACUC) at the University of Colorado Anschutz Medical Campus protocol #00316 and were performed using accepted veterinary standards. The University of Colorado Anschutz Medical Campus is AAALAC accredited; and its facilities meet and adhere to the standards in the "Guide for the Care and Use of Laboratory Animals". All mice were purchased from Charles River Laboratories (CD1) and housed in pathogen-free, biosafety level-2 animal facilities.

***In vivo* transposon screening.** Triplicate cultures of the pooled CJB111 pKrmit transposon library (*29*) were grown overnight at 37˚C in THB with kanamycin at 300 µg/mL and back diluted to an OD600 0.4. Libraries were normalized to ~4 x 10^7 CFU/100 µL and injected via

tail-vein into 6–8-week-old CD-1 male mice using the established hematogenous infection model (*96-99*). Blood was collected by cardiac puncture between ~18-28 hours post infection. 100 µL of input library and blood was plated in duplicated on CHROMagar Strep B with 300 µg/mL kanamycin and incubated overnight at 37˚C to collect recovered transposon mutants. Bacterial growth from spread plates were collected and 3-4 mice per library were pooled together, genomic DNA extracted using ZymoBiomics DNA miniprep Kit (Zymo Research).

Transposon library sequencing. Libraries were prepared and sequenced at the University of Minnesota Genomics Center (UMGC) according to https://www.protocols.io/view/transposon-insertion-sequencing-tn-seq-library-pre-rm7vzn6d5vx1/v1. Briefly, genomic DNA was enzymatically fragmented, and adapters added using the NEB Ultra II FS kit (New England Biolabs), and ~50 ng of fragmented adapted gDNA was used as a template for enrichment by PCR (16 cycles) for the transposon insertions using mariner-specific (TCGTCGGCAGCGTCAGATGTGTATAAGAGACAGCCGGGGACTTATCATCCAACC) and Illumina P7 primers. The enriched PCR products were diluted to 1ng/ul and 10 ul was used as a template for an indexing PCR (9 cycles) using Nextera_R1 (iP5) and Nextera_R2 (iP7) primers. Sequencing was performed using 150- base paired-end format on an Illumina NextSeq 2000 and Illumina NovaSeq 6000 system to generate ~40-60 million reads per library.

Tn-sequencing analysis. The R1 reads from both sequencing runs were concatenated and quality was assessed using FastQC (*100*)(http://www.bioinformatics.babraham.ac.uk/projects/fastqc/). Reads were trimmed using Cutadapt (v 4.2) (*101*) with the following parameters; sequence length with a minimum of 12

bases, removal of flanking "N" bases, reads were trimmed of 3' "G" bases, and reads were trimmed with the reverse complemented mariner transposon sequence (ACTTATCAGCCAACCTGTTA). TRANSIT (v 3.2.7) (*102*) was used to align trimmed reads to the CJB111 genome (CP063198) and for analysis of transposon insertion sites. The Transit PreProcessor processed reads using default parameters with the Sassetti protocol, no primer sequence, and mapped to the genome sequence using Burrows-Wheeler Alignment (BWA) (*103*). Insertion sites were normalized using the Total Trimmed Reads (TTR) method in TRANSIT and analyzed using the resampling method to compare the insertion counts recovered in blood vs the input library using default parameters, with the addition of ignoring TA sites within 5% of the 5' and 3' end of the gene. All sequencing reads have been deposited into NCBI SRA under BioProject ID PRJNA1125445.

Murine model of bloodstream infection. We infected mice as previously described (*96-99*). Briefly, 8-week-old CD1 male mice were intravenously challenged with 1 x 10^7 CFU GBS. At 12, 24, and/or 48 h post-infection, blood samples were taken by tail prick and plated on THA to quantify GBS CFU burden. At time-of-death or 72 h post-infection mice were sacrificed, and blood was harvested by cardiac puncture and lung and heart tissue were removed and homogenized in sterile PBS. All samples were plated on THA or CHROMagar to quantify GBS CFU burden. For neutrophil depletion, mice were given 200µg *InVivo*MAb anti-mouse Ly6G antibody (Bio X Cell, Lebanon, NH) or 200µg *InVivo*MAb rat IgG2a isotype control diluted in *InVivo*Pure pH 7.0 dilution buffer by intraperitoneal injection 24 h before infection.

GloA protein comparisons. GloA amino acid sequences where aligned using ClustalOmega (*104*) and the alignment figure was created using the ESPript Server (*105*)(https://espript.ibcp.fr). Protein IDs used: ABA45143.1 (GBS A909), QOW77196.1 (GBS CJB111), WP_001116201.1 (GBS COH1), WP_002985686.1 (GAS 5448), WP_003722292.1 (*L. monocytogenes* 10403S), and P0AC81.1 (*E. coli* K-12). GBS GloA phylogenetic tree was generated using NCBI BlastP (*106, 107*) and visualized using FigTree v1.4.4 (http://tree.bio.ed.ac.uk/software/figtree/). The protein ID QOW77196.1 (GBS CJB111) was used as the query against *S. agalactiae* and only proteins with percent identity and query cover greater than 50% are shown. The dimeric structure of the *S. agalactiae* GloA was predicted using AlphaFold2 (*108*) as implemented in ColabFold (*109*). PyMOL (version 2.5.2, Schrödinger, LLC.) was used to create images of the predicted GloA structure and the *E. coli* glyoxalase I crystal structure RCSB PDB entry 19FZ (*66, 110*)(RCSB.org).

***In vitro* growth comparisons.** Overnight cultures of Streptococcal strains were diluted 1:100 in mCDM with or without methylglyoxal (MG, Sigma-Aldrich M0252, St. Louis, MO) or hydrogen peroxide 3% w/w (VWR, Radnor, PA) at concentrations listed in figure legends in a 96-well plate. For strain/serotype comparisons with MG, the plate was incubated at 37°C without shaking and OD600 readings were taken at 0, 6, and 24 hrs. Percent growth was calculated by dividing the average OD600 with MG to the average OD600 no MG control for each strain. MICs were determined for each strain by MG concentrations that had <5% growth at 24 hrs. For 24 hr growth curves with MG, the plate was covered with a Breathe-Easy gas permeable sealing membrane (USA Scientific, Ocala, FL) and then incubated at 37°C without shaking in a Tecan Infinite M Plex for 24 h with OD600 taken every 30 min. For growth curves with hydrogen

peroxide, the plate was incubated at 37°C without shaking and samples were taken every 2 hrs for dilution plating on THA.

ELISAs on culture pellets. Overnight cultures of Streptococcal strains were diluted 1:100 in mCDM and then grown for 4 h at 37°C. 3 mL of each culture was pelleted, re-suspended in PBS, and then homogenized using 0.1 mm dia. Zirconia beads. Methylglyoxal concentration in culture samples was measured using an ELISA kit (Biomatik EKN53482, Kitchener, ON, CA) per manufacture instructions. BSA protein assay standard was used to quantify protein concentration in each culture sample.

RT-qPCR. Samples were made by centrifuging 1 mL aliquots of cultures grown to mid-log phase in mCDM and then re-suspending in 1 mL fresh mCDM and incubating for 30 min at 37°C. 1 mL of RNAProtect Bacteria Reagent (Qiagen, Venlo, NL) was then added before centrifuging and washing pellets with ice cold PBS. Sample RNA was prepped using the NucleoSpin RNA kit (Macherey-Nagel, Dueren, DE) and TURBO DNase treated (Invitrogen by Thermo Fisher, Waltham, MA) per manufacture instructions. 250 ng of RNA was made into cDNA for each sample using the qScript cDNA Synthesis Kit (Quantabio, Beverly, MA) per manufacture instructions. cDNA was then diluted 1:20 in water and RT-qPCR run using PerfeCTa SYBR Green FastMix (Quantabio, Beverly, MA) per manufacture instructions and *glcK*, *gloA*, and *gloB* qPCR primers (see Table S2). Each sample was run in technical duplicate for each gene. Each sample Cq value for *glcK*, *gloA*, and *gloB* was normalized to the total average CJB111 Cq value for each gene, respectively.

Hemolysis assay. Overnight cultures of Streptococcal strains were diluted 1:100 in THB and then grown to mid-log phase at 37°C. Cultures were then normalized to OD600 0.4 in PBS. 400 µL blood, 400 µL PBS, and 200 µL normalized culture was added to each sample microfuge tube. 400 µL blood and 600 µL sterile water was added to positive control tubes and 400 µL blood and 600 µL PBS was added to negative control tubes. Tubes were made in technical duplicate and incubated at 37°C with rotation. At 24 hrs, 100 µL aliquots were taken and centrifuged at 5500 x g for 1 min. OD543 of supernatant was measured using a Tecan Infinite M Plex and %lysis calculated by subtracting negative control from all samples and then dividing samples by positive controls.

Neutrophil opsonophagocytic killing. HL60 cells were cultured in RPMI + 10% FBS, differentiated with 1.25% DMSO for 4 days, and infected as previously described (*111*). HL60 cells were infected at an MOI of 0.002 and incubated, at 37°C with shaking, for 5 hrs. %Survival at 5 hrs was calculated by dividing CFU recovered from wells with GBS opsonized with normal serum by CFU recovered from wells with GBS opsonized with heat-killed (HK) serum. CFU from control wells without HL60s were also quantified.

Flow cytometry detection of methylglyoxal-modified proteins in HL60 cells. To determine the impact of infection on methylglyoxal levels in neutrophil-like cells, differentiated Hl60s were first re-suspended in fresh RPMI + 10%FBS with 0 or 20mM glucose and allowed to equilibrate for 2 hrs. 1 mL aliquots of differentiated HL60 cells were infected with GBS at MOI 20 for 2.5 hours and then harvested by centrifugation (500 x g) and stained using eBioscience Fixable Viability Dye eFluor 506 (Catalog # 65-0866-18) in PBS for 30 minutes at room temperature.

Cells were then stained with anti-human Cd11b antibody conjugated to FITC (1:20 dilution; BD Biosciences 562793) in MACS buffer for 30 minutes at room temperature and were fixed and permeabilized using the FoxP3 fixation/permeabilization kit (Thermo Fisher Scientific, Catalog # 00-5523-00) according to manufacturer's instructions. Cells were then stained for intracellular methylglyoxal using an anti-MG antibody conjugated to PE (clone 9E7; Cat # MA5-45812; recognizes methylglyoxal-modified proteins) or an IgG2a isotype control (Cat # MG2A04) at final concentrations of 0.67 ug/mL (30 minutes in permeabilization buffer at room temperature). Stained cells were run on a BD LSRFortessa (BD Biosciences) using the BD FacsDiva software (v9) and analyzed by BD FlowJo software (v10.8). Gating strategy was determined by fluorescence minus one (FMO) controls.

Statistical analysis. Statistical analysis was performed using Prism version 10.1 for Windows (GraphPad Software, San Diego, CA, USA) as described in figure legends.

Acknowledgements

We would like to thank Dr. Jeffrey Kavanaugh from the University of Colorado Anschutz Medical Campus for help with protein modeling. The work was supported by the American Heart Association grant 23POST1013835 to L.R.J, and the National Institutes of Health grants R01NS116716 and R01AI153332 to K.S.D. and grant F31AI178881 to M.S.A.

Figures

Figure 1. *In vivo* transposon mutant sequencing of GBS survival in the blood. (A) CIRCOS atlas representation of GBS CJB111 genome is shown with base pair ruler on the outer ring. The inner ring in blue shows $\log_2$FC (0 to -5/max) of significantly underrepresented genes ($P_{adj} < 0.05$). The next inner ring in pink shows $\log_2$FC (0 to 5/max) of significantly overrepresented genes ($P_{adj} < 0.05$). The most inner ring in grey denotes genes with $P_{adj} < 0.001$. Underrepresented genes or operons of interest are labeled in the center (also listed in Table 1). (B) Clusters of orthologous genes (COG) assignments for significant gene hits normalized to the total number of GBS genes in each COG. The total number of significant genes in each COG are in parentheses. (C) Diagram of the glyoxalase pathway for methylglyoxal (MG) breakdown. Significance determined by (A&B) TRANSIT analysis and Trimmed Total Reads (TTR) normalization with $P_{adj} < 0.05$ and Log_2 Fold Change < -2 or > 2.

Table 1. Important GBS virulence factors contribute to survival in blood.

Figure 2. MG resistance differs across GBS isolates. Percent growth of representative serotype Ia, Ib, III, and V GBS strains and *S. pyogenes* 5448 (GAS) with 1.0 mM MG in mCDM at 6 hrs.

Figure 3. Characterization of GBS glyoxalase A protein. (A) Alignment of GloA amino acid sequences from GBS CJB111, GBS A909, GBS COH1, *S. pyogenes* 5448, *L. monocytogenes* 10403S, and *E. coli* K-12. Green stars indicate known or predicted metal binding sites and colored bar indicates confidence of structure prediction. (B) Phylogenetic tree for 57 GBS GloA proteins. Proteins/branches with a mutation in amino acid residue A45 are labeled and colored. Red indicates an A45S mutation, purple indicates an A45T mutation, and grey indicates a

mutation that only occurred once. (C) Left: Solved tertiary protein structure for *E. coli* K-12 GloA. The grey spheres are Nickel 2+ ions. Middle: AlphaFold2 predicted tertiary protein structure for GBS A909/CJB111 GloA. The purple spheres indicate the A45 residue. Right: Superimposed tertiary structures for *E. coli* GloA and GBS GloA. (D) Left: Predicted tertiary protein dimer for GBS A909/CJB111 GloA. Right: 180° horizontal rotation of the predicted tertiary protein dimer with the blue monomer containing GBS COH1 A45S mutation. Black arrows indicate predicted active site.

Figure 4. The contribution of glyoxalase A to GBS methylglyoxal detoxification. (A) ELISA MG quantification of cell pellets for WT CJB111, Δ*gloA*, and p*gloA* strains after growth in mCDM for 4 hours. (B) Growth curve measured by OD_{600} for WT CJB111, Δ*gloA*, and p*gloA* strains grown with or without 0.5 mM MG in mCDM. (C) Comparison of growth shown in (B) at 8hrs between strains. Significance determined by (A) Student *t* test or (C) 2way ANOVA with Šídák's multiple comparisons test with $P < 0.05$. * < 0.05, ** < 0.01, *** < 0.001, **** < 0.0001.

Figure 5. Methylglyoxal detoxification is necessary for GBS infection. (A) Survival curve of mice tail-vein injected with 10^7 CFU WT CJB111 or Δ*gloA*. (B) Recovered CFU counts from the blood of infected mice at 24 and 48 hours post-infection. (C) Recovered CFU counts from the blood, heart, and lungs of infected mice at time-of-death. Significance determined by (A) Log-rank (Mantel-Cox) test or (B&C) Mann-Whitney *U* test with $P < 0.05$. * < 0.05, ** < 0.01.

Figure 6. Methylglyoxal detoxification is necessary for GBS survival against neutrophil-like HL-60 cells. (A) Survival of WT CJB111, Δ*gloA*, and p*gloA* strains after 5 hours infection of HL60-neutrophils. (B) Flow cytometry quantification of intracellular MG-modified proteins in HL60-neutrophils with or without WT CJB111 infection. Left: Representative histogram displaying MG signal that includes isotype control, uninfected, and infected cells. Right: MFI quantification for MG in uninfected and infected samples. (C) Survival curve of normal or neutrophil depleted mice that were tail-vein injected with 10^7 CFU WT CJB111 Δ*gloA*. (D) Recovered CFU counts from the blood of infected mice 12 hours post-infection. Significance determined by (A&B) Unpaired Student *t* test, (C) Log-rank (Mantel-Cox) test, or (D) One-way ANOVA with Holm-Šídák's multiple comparisons test with $P < 0.05$. * < 0.05, ** < 0.01, *** < 0.001, **** < 0.0001.

Supplementary Material

Table S1. Complete *in vivo* blood Tn-sequencing dataset.

Table S2. Primers and Strains

Figure S1. idDT confidence score across GBS GloA predicted structure.

Figure S2. Transcription of the glyoxalase pathway. (A) Baseline transcription of *gloA* and *gloB* genes grown to mid-log in mCDM and quantified by RT-qPCR. Gene transcript levels were

normalized to the average CJB111 levels. Significance determined by 2way ANOVA with $P < 0.05$. * < 0.05.

Figure S3. The impact of Glyoxalase A GBS growth and virulence. Growth curves for CJB111, Δ*gloA*, and p*gloA* strains in mCDM with (A) 10, 22, or 50 mM glucose quantified by OD_{600} or (B) 0.1% (29.4mM) hydrogen peroxide quantified by CFU enumeration. (C) Percent red blood cell lysis of human blood for CJB111, Δ*gloA*, and p*gloA* strains relative to positive lysis control at 24hrs post-inoculation.

Figure S4. The impact of serum and glucose on neutrophil survival assays. (A) Survival of CJB111, Δ*gloA*, and p*gloA* strains over time in the presence of serum without neutrophils. Percent survival was calculated by dividing CFU recovered from wells with GBS opsonized with normal serum by CFU recovered from wells with GBS opsonized with heat-killed (HK) serum. (B) Flow cytometry quantification of intracellular MG-modified proteins in HL60-neutrophils with or without WT CJB111 infection and 0mM glucose media. Left: Representative histogram displaying MG signal that includes isotype control, uninfected, and infected cells. Right: MFI quantification for MG in uninfected and infected samples.

References

1. K. S. Doran, V. Nizet, Molecular pathogenesis of neonatal group B streptococcal infection: no longer in its infancy. *Mol Microbiol* **54**, 23-31 (2004).
2. L. K. Francois Watkins *et al.*, Epidemiology of Invasive Group B Streptococcal Infections Among Nonpregnant Adults in the United States, 2008-2016. *JAMA Intern Med* **179**, 479-488 (2019).

3. A. A. El-Gendy *et al.*, Serotyping and Antibiotic Susceptibility of Invasive Streptococcus agalactiae in Egyptian Patients with or without Diabetes Mellitus. *Am J Trop Med Hyg* **105**, 1684-1689 (2021).
4. M. S. Edwards *et al.*, Long-term sequelae of group B streptococcal meningitis in infants. *J Pediatr* **106**, 717-722 (1985).
5. R. Libster *et al.*, Long-term outcomes of group B streptococcal meningitis. *Pediatrics* **130**, e8-15 (2012).
6. J. Hall *et al.*, Maternal Disease With Group B Streptococcus and Serotype Distribution Worldwide: Systematic Review and Meta-analyses. *Clin Infect Dis* **65**, S112-S124 (2017).
7. N. K. Kurian, D. Modi, Mechanisms of group B Streptococcus-mediated preterm birth: lessons learnt from animal models. *Reprod Fertil* **3**, R109-R120 (2022).
8. A. Berardi *et al.*, Understanding Factors in Group B Streptococcus Late-Onset Disease. *Infect Drug Resist* **14**, 3207-3218 (2021).
9. E. M. Sabroske *et al.*, Evolving antibiotic resistance in Group B Streptococci causing invasive infant disease: 1970-2021. *Pediatr Res* **93**, 2067-2071 (2023).
10. J. Vornhagen, K. M. Adams Waldorf, L. Rajagopal, Perinatal Group B Streptococcal Infections: Virulence Factors, Immunity, and Prevention Strategies. *Trends Microbiol* **25**, 919-931 (2017).
11. H. S. Manzer *et al.*, The Group B Streptococcal Adhesin BspC Interacts with Host Cytokeratin 19 To Promote Colonization of the Female Reproductive Tract. *mBio* **13**, e0178122 (2022).
12. B. L. Spencer *et al.*, A type VII secretion system in Group B Streptococcus mediates cytotoxicity and virulence. *PLoS Pathog* **17**, e1010121 (2021).
13. L. Mereghetti, I. Sitkiewicz, N. M. Green, J. M. Musser, Extensive adaptive changes occur in the transcriptome of Streptococcus agalactiae (group B streptococcus) in response to incubation with human blood. *PLoS One* **3**, e3143 (2008).
14. M. S. Akbari, K. S. Doran, L. R. Burcham, Metal Homeostasis in Pathogenic Streptococci. *Microorganisms* **10**, (2022).
15. Y. Liu, J. Liu, Group B Streptococcus: Virulence Factors and Pathogenic Mechanism. *Microorganisms* **10**, (2022).
16. B. Spellerberg *et al.*, Identification of genetic determinants for the hemolytic activity of Streptococcus agalactiae by ISS1 transposition. *J Bacteriol* **181**, 3212-3219 (1999).
17. K. S. Doran, G. Y. Liu, V. Nizet, Group B streptococcal beta-hemolysin/cytolysin activates neutrophil signaling pathways in brain endothelium and contributes to development of meningitis. *J Clin Invest* **112**, 736-744 (2003).
18. A. Ring *et al.*, Group B streptococcal beta-hemolysin induces mortality and liver injury in experimental sepsis. *J Infect Dis* **185**, 1745-1753 (2002).
19. G. Y. Liu *et al.*, Sword and shield: linked group B streptococcal beta-hemolysin/cytolysin and carotenoid pigment function to subvert host phagocyte defense. *Proc Natl Acad Sci U S A* **101**, 14491-14496 (2004).
20. M. E. Hensler *et al.*, Virulence role of group B Streptococcus beta-hemolysin/cytolysin in a neonatal rabbit model of early-onset pulmonary infection. *J Infect Dis* **191**, 1287-1291 (2005).
21. M. J. Cieslewicz *et al.*, Structural and genetic diversity of group B streptococcus capsular polysaccharides. *Infect Immun* **73**, 3096-3103 (2005).

22. K. Noble *et al.*, Group B Streptococcus cpsE Is Required for Serotype V Capsule Production and Aids in Biofilm Formation and Ascending Infection of the Reproductive Tract during Pregnancy. *ACS Infect Dis* **7**, 2686-2696 (2021).
23. A. Schuchat, Epidemiology of group B streptococcal disease in the United States: shifting paradigms. *Clin Microbiol Rev* **11**, 497-513 (1998).
24. L. Madrid *et al.*, Infant Group B Streptococcal Disease Incidence and Serotypes Worldwide: Systematic Review and Meta-analyses. *Clin Infect Dis* **65**, S160-S172 (2017).
25. H. J. Jennings, C. Lugowski, D. L. Kasper, Conformational aspects critical to the immunospecificity of the type III group B streptococcal polysaccharide. *Biochemistry* **20**, 4511-4518 (1981).
26. M. S. Edwards, D. L. Kasper, H. J. Jennings, C. J. Baker, A. Nicholson-Weller, Capsular sialic acid prevents activation of the alternative complement pathway by type III, group B streptococci. *J Immunol* **128**, 1278-1283 (1982).
27. J. Hayrinen, S. Pelkonen, J. Finne, Structural similarity of the type-specific group B streptococcal polysaccharides and the carbohydrate units of tissue glycoproteins: evaluation of possible cross-reactivity. *Vaccine* **7**, 217-224 (1989).
28. B. L. Spencer, A. Chatterjee, B. A. Duerkop, C. J. Baker, K. S. Doran, Complete Genome Sequence of Neonatal Clinical Group B Streptococcal Isolate CJB111. *Microbiol Resour Announc* **10**, (2021).
29. L. R. Burcham *et al.*, Genomic Analyses Identify Manganese Homeostasis as a Driver of Group B Streptococcal Vaginal Colonization. *mBio* **13**, e0098522 (2022).
30. L. R. Burcham *et al.*, Identification of Zinc-Dependent Mechanisms Used by Group B Streptococcus To Overcome Calprotectin-Mediated Stress. *mBio* **11**, (2020).
31. J. Morgenstern, M. Campos Campos, P. Nawroth, T. Fleming, The Glyoxalase System-New Insights into an Ancient Metabolism. *Antioxidants (Basel)* **9**, (2020).
32. Y. Inoue, A. Kimura, Methylglyoxal and regulation of its metabolism in microorganisms. *Adv Microb Physiol* **37**, 177-227 (1995).
33. C. Poyart *et al.*, Attenuated virulence of Streptococcus agalactiae deficient in D-alanyl-lipoteichoic acid is due to an increased susceptibility to defensins and phagocytic cells. *Mol Microbiol* **49**, 1615-1625 (2003).
34. Q. Cheng, D. Stafslien, S. S. Purushothaman, P. Cleary, The group B streptococcal C5a peptidase is both a specific protease and an invasin. *Infect Immun* **70**, 2408-2413 (2002).
35. S. Dramsi *et al.*, Assembly and role of pili in group B streptococci. *Mol Microbiol* **60**, 1401-1413 (2006).
36. K. S. Doran *et al.*, Blood-brain barrier invasion by group B Streptococcus depends upon proper cell-surface anchoring of lipoteichoic acid. *J Clin Invest* **115**, 2499-2507 (2005).
37. C. Whidbey *et al.*, A hemolytic pigment of Group B Streptococcus allows bacterial penetration of human placenta. *J Exp Med* **210**, 1265-1281 (2013).
38. E. Boldenow *et al.*, Group B Streptococcus circumvents neutrophils and neutrophil extracellular traps during amniotic cavity invasion and preterm labor. *Sci Immunol* **1**, (2016).
39. S. Papasergi *et al.*, The GBS PI-2a pilus is required for virulence in mice neonates. *PLoS One* **6**, e18747 (2011).
40. K. A. Patras *et al.*, Group B Streptococcus Biofilm Regulatory Protein A Contributes to Bacterial Physiology and Innate Immune Resistance. *J Infect Dis* **218**, 1641-1652 (2018).

41. V. Mercado-Evans *et al.*, Gestational diabetes augments group B Streptococcus infection by disrupting maternal immunity and the vaginal microbiota. *Nat Commun* **15**, 1035 (2024).
42. A. F. Carlin *et al.*, Group B Streptococcus suppression of phagocyte functions by protein-mediated engagement of human Siglec-5. *J Exp Med* **206**, 1691-1699 (2009).
43. S. Uchiyama *et al.*, Dual actions of group B Streptococcus capsular sialic acid provide resistance to platelet-mediated antimicrobial killing. *Proc Natl Acad Sci U S A* **116**, 7465-7470 (2019).
44. P. Moulin *et al.*, The Adc/Lmb System Mediates Zinc Acquisition in Streptococcus agalactiae and Contributes to Bacterial Growth and Survival. *J Bacteriol* **198**, 3265-3277 (2016).
45. M. S. Akbari *et al.*, The impact of nutritional immunity on Group B streptococcal pathogenesis during wound infection. *mBio*, e0030423 (2023).
46. A. Clancy *et al.*, Evidence for siderophore-dependent iron acquisition in group B streptococcus. *Mol Microbiol* **59**, 707-721 (2006).
47. S. Shabayek, R. Bauer, S. Mauerer, B. Mizaikoff, B. Spellerberg, A streptococcal NRAMP homologue is crucial for the survival of Streptococcus agalactiae under low pH conditions. *Mol Microbiol* **100**, 589-606 (2016).
48. M. J. Sullivan, K. G. K. Goh, D. Gosling, L. Katupitiya, G. C. Ulett, Copper Intoxication in Group B Streptococcus Triggers Transcriptional Activation of the cop Operon That Contributes to Enhanced Virulence during Acute Infection. *J Bacteriol* **203**, e0031521 (2021).
49. C. Faralla *et al.*, Analysis of two-component systems in group B Streptococcus shows that RgfAC and the novel FspSR modulate virulence and bacterial fitness. *mBio* **5**, e00870-00814 (2014).
50. L. Thomas, L. Cook, Two-Component Signal Transduction Systems in the Human Pathogen Streptococcus agalactiae. *Infect Immun* **88**, (2020).
51. D. S. Ipe *et al.*, Discovery and Characterization of Human-Urine Utilization by Asymptomatic-Bacteriuria-Causing Streptococcus agalactiae. *Infect Immun* **84**, 307-319 (2016).
52. C. Poyart, M. C. Lamy, C. Boumaila, F. Fiedler, P. Trieu-Cuot, Regulation of D-alanyl-lipoteichoic acid biosynthesis in Streptococcus agalactiae involves a novel two-component regulatory system. *J Bacteriol* **183**, 6324-6334 (2001).
53. D. Quach *et al.*, The CiaR response regulator in group B Streptococcus promotes intracellular survival and resistance to innate immune defenses. *J Bacteriol* **191**, 2023-2032 (2009).
54. Y. Yang *et al.*, Role of Two-Component System Response Regulator bceR in the Antimicrobial Resistance, Virulence, Biofilm Formation, and Stress Response of Group B Streptococcus. *Front Microbiol* **10**, 10 (2019).
55. S. Khosa, Z. AlKhatib, S. H. Smits, NSR from Streptococcus agalactiae confers resistance against nisin and is encoded by a conserved nsr operon. *Biol Chem* **394**, 1543-1549 (2013).
56. S. Khosa *et al.*, Structural basis of lantibiotic recognition by the nisin resistance protein from Streptococcus agalactiae. *Sci Rep* **6**, 18679 (2016).
57. L. Rajagopal, A. Vo, A. Silvestroni, C. E. Rubens, Regulation of purine biosynthesis by a eukaryotic-type kinase in Streptococcus agalactiae. *Mol Microbiol* **56**, 1329-1346 (2005).

58. G. S. Tamura, A. Nittayajarn, D. L. Schoentag, A glutamine transport gene, glnQ, is required for fibronectin adherence and virulence of group B streptococci. *Infect Immun* **70**, 2877-2885 (2002).
59. D. S. Ipe *et al.*, Conserved bacterial de novo guanine biosynthesis pathway enables microbial survival and colonization in the environmental niche of the urinary tract. *ISME J* **15**, 2158-2162 (2021).
60. I. Santi *et al.*, CsrRS regulates group B Streptococcus virulence gene expression in response to environmental pH: a new perspective on vaccine development. *J Bacteriol* **191**, 5387-5397 (2009).
61. Q. Yang, M. Zhang, D. J. Harrington, G. W. Black, I. C. Sutcliffe, A proteomic investigation of Streptococcus agalactiae reveals that human serum induces the C protein beta antigen and arginine deiminase. *Microbes Infect* **13**, 757-760 (2011).
62. I. van de Rijn, R. E. Kessler, Growth characteristics of group A streptococci in a new chemically defined medium. *Infect Immun* **27**, 444-448 (1980).
63. M. M. Zhang, C. L. Ong, M. J. Walker, A. G. McEwan, Defence against methylglyoxal in Group A Streptococcus: a role for Glyoxylase I in bacterial virulence and survival in neutrophils? *Pathog Dis* **74**, (2016).
64. A. Anaya-Sanchez, Y. Feng, J. C. Berude, D. A. Portnoy, Detoxification of methylglyoxal by the glyoxalase system is required for glutathione availability and virulence activation in Listeria monocytogenes. *PLoS Pathog* **17**, e1009819 (2021).
65. M. J. MacLean, L. S. Ness, G. P. Ferguson, I. R. Booth, The role of glyoxalase I in the detoxification of methylglyoxal and in the activation of the KefB K+ efflux system in Escherichia coli. *Mol Microbiol* **27**, 563-571 (1998).
66. M. M. He, S. L. Clugston, J. F. Honek, B. W. Matthews, Determination of the structure of Escherichia coli glyoxalase I suggests a structural basis for differential metal activation. *Biochemistry* **39**, 8719-8727 (2000).
67. K. H. Darwin, S. A. Stanley, The aldehyde hypothesis: metabolic intermediates as antimicrobial effectors. *Open Biol* **12**, 220010 (2022).
68. G. Limon, N. M. Samhadaneh, A. Pironti, K. H. Darwin, Aldehyde accumulation in Mycobacterium tuberculosis with defective proteasomal degradation results in copper sensitivity. *mBio* **14**, e0036323 (2023).
69. H. Rachman *et al.*, Critical role of methylglyoxal and AGE in mycobacteria-induced macrophage apoptosis and activation. *PLoS One* **1**, e29 (2006).
70. S. W. T. Lai, E. J. Lopez Gonzalez, T. Zoukari, P. Ki, S. C. Shuck, Methylglyoxal and Its Adducts: Induction, Repair, and Association with Disease. *Chem Res Toxicol* **35**, 1720-1746 (2022).
71. J. M. Daley, A. A. Thomay, M. D. Connolly, J. S. Reichner, J. E. Albina, Use of Ly6G-specific monoclonal antibody to deplete neutrophils in mice. *J Leukoc Biol* **83**, 64-70 (2008).
72. R. L. Goldenberg, J. C. Hauth, W. W. Andrews, Intrauterine infection and preterm delivery. *N Engl J Med* **342**, 1500-1507 (2000).
73. T. A. Hooven *et al.*, The Streptococcus agalactiae Stringent Response Enhances Virulence and Persistence in Human Blood. *Infect Immun* **86**, (2018).
74. L. Mereghetti, I. Sitkiewicz, N. M. Green, J. M. Musser, Identification of an unusual pattern of global gene expression in group B Streptococcus grown in human blood. *PLoS One* **4**, e7145 (2009).

75. B. Di Palo *et al.*, Adaptive response of Group B streptococcus to high glucose conditions: new insights on the CovRS regulation network. *PLoS One* **8**, e61294 (2013).
76. Y. Lopez *et al.*, Serotype, virulence profile, antimicrobial resistance and macrolide-resistance determinants in Streptococcus agalactiae isolates in pregnant women and neonates in Catalonia, Spain. *Enferm Infecc Microbiol Clin (Engl Ed)* **36**, 472-477 (2018).
77. X. Zhang, C. G. Schalkwijk, K. Wouters, Immunometabolism and the modulation of immune responses and host defense: A role for methylglyoxal? *Biochim Biophys Acta Mol Basis Dis* **1868**, 166425 (2022).
78. P. J. Beisswenger, Methylglyoxal in diabetes: link to treatment, glycaemic control and biomarkers of complications. *Biochem Soc Trans* **42**, 450-456 (2014).
79. C. Lee, C. Park, Bacterial Responses to Glyoxal and Methylglyoxal: Reactive Electrophilic Species. *Int J Mol Sci* **18**, (2017).
80. S. L. Hazen, F. F. Hsu, A. d'Avignon, J. W. Heinecke, Human Neutrophils Employ Myeloperoxidase To Convert a-Amino Acids to a Batter of Reactive Aldehydes: A Pathway for Aldehyde Generation at Sites of Inflammation. *Biochemistry* **37**, 6864-6873 (1998).
81. A. Furuta *et al.*, Bacterial and Host Determinants of Group B Streptococcal Infection of the Neonate and Infant. *Front Microbiol* **13**, 820365 (2022).
82. S. L. Clugston, R. Yajima, J. F. Honek, Investigation of metal binding and activation of Escherichia coli glyoxalase I: kinetic, thermodynamic and mutagenesis studies. *Biochem J* **377**, 309-316 (2004).
83. U. Suttisansanee *et al.*, Structural variation in bacterial glyoxalase I enzymes: investigation of the metalloenzyme glyoxalase I from Clostridium acetobutylicum. *J Biol Chem* **286**, 38367-38374 (2011).
84. L. Zeng, P. Noeparvar, R. A. Burne, B. S. Glezer, Genetic characterization of glyoxalase pathway in oral streptococci and its contribution to interbacterial competition. *J Oral Microbiol* **16**, 2322241 (2024).
85. L. C. C. Cook, H. Hu, M. Maienschein-Cline, M. J. Federle, A Vaginal Tract Signal Detected by the Group B Streptococcus SaeRS System Elicits Transcriptomic Changes and Enhances Murine Colonization. *Infect Immun* **86**, (2018).
86. M. Alfano, C. Cavazza, Structure, function, and biosynthesis of nickel-dependent enzymes. *Protein Sci* **29**, 1071-1089 (2020).
87. T. Eitinger, M. A. Mandrand-Berthelot, Nickel transport systems in microorganisms. *Arch Microbiol* **173**, 1-9 (2000).
88. N. Krymkiewicz, E. Dieguez, U. D. Rekarte, N. Zwaig, Properties and mode of action of a bactericidal compound (=methylglyoxal) produced by a mutant of Escherichia coli. *J Bacteriol* **108**, 1338-1347 (1971).
89. K. Takahashi, Further studies on the reactions of phenylglyoxal and related reagents with proteins. *J Biochem* **81**, 403-414 (1977).
90. K. Takahashi, The reactions of phenylglyoxal and related reagents with amino acids. *J Biochem* **81**, 395-402 (1977).
91. S. T. Cheung, M. L. Fonda, Kinetics of the inactivation of Escherichia coli glutamate apodecarboxylase by phenylglyoxal. *Arch Biochem Biophys* **198**, 541-547 (1979).

92. N. Rabbani, P. J. Thornalley, Measurement of methylglyoxal by stable isotopic dilution analysis LC-MS/MS with corroborative prediction in physiological samples. *Nat Protoc* **9**, 1969-1979 (2014).
93. C. G. Schalkwijk, C. D. A. Stehouwer, Methylglyoxal, a Highly Reactive Dicarbonyl Compound, in Diabetes, Its Vascular Complications, and Other Age-Related Diseases. *Physiol Rev* **100**, 407-461 (2020).
94. R. A. Keogh *et al.*, Group B Streptococcus adaptation promotes survival in a hyperinflammatory diabetic wound environment. *Sci Adv* **8**, eadd3221 (2022).
95. S. Kant, L. Liu, A. Vazquez-Torres, The methylglyoxal pathway is a sink for glutathione in Salmonella experiencing oxidative stress. *PLoS Pathog* **19**, e1011441 (2023).
96. L. R. Joyce *et al.*, Identification of a novel cationic glycolipid in Streptococcus agalactiae that contributes to brain entry and meningitis. *PLoS Biol* **20**, e3001555 (2022).
97. A. Banerjee *et al.*, Bacterial Pili exploit integrin machinery to promote immune activation and efficient blood-brain barrier penetration. *Nat Commun* **2**, 462 (2011).
98. B. J. Kim *et al.*, Bacterial induction of Snail1 contributes to blood-brain barrier disruption. *J Clin Invest* **125**, 2473-2483 (2015).
99. B. L. Spencer *et al.*, Cas9 Contributes to Group B Streptococcal Colonization and Disease. *Front Microbiol* **10**, 1930 (2019).
100. S. W. Wingett, S. Andrews, FastQ Screen: A tool for multi-genome mapping and quality control. *F1000Res* **7**, 1338 (2018).
101. M. Martin, Cutadapt removes adapter sequences from high-throughput sequencing reads. 2011 (10.14806/ej.17.1.200).
102. M. A. DeJesus, C. Ambadipudi, R. Baker, C. Sassetti, T. R. Ioerger, TRANSIT--A Software Tool for Himar1 TnSeq Analysis. *PLoS Comput Biol* **11**, e1004401 (2015).
103. H. Li, R. Durbin, Fast and accurate short read alignment with Burrows-Wheeler transform. *Bioinformatics* **25**, 1754-1760 (2009).
104. F. Madeira *et al.*, Search and sequence analysis tools services from EMBL-EBI in 2022. *Nucleic Acids Res* **50**, W276-W279 (2022).
105. X. Robert, P. Gouet, Deciphering key features in protein structures with the new ENDscript server. *Nucleic Acids Res* **42**, W320-324 (2014).
106. S. F. Altschul *et al.*, Gapped BLAST and PSI-BLAST: a new generation of protein database search programs. *Nucleic Acids Res* **25**, 3389-3402 (1997).
107. S. F. Altschul *et al.*, Protein database searches using compositionally adjusted substitution matrices. *FEBS J* **272**, 5101-5109 (2005).
108. J. Jumper *et al.*, Highly accurate protein structure prediction with AlphaFold. *Nature* **596**, 583-589 (2021).
109. M. Mirdita *et al.*, ColabFold: making protein folding accessible to all. *Nat Methods* **19**, 679-682 (2022).
110. H. M. Berman *et al.*, The Protein Data Bank. *Nucleic Acids Res* **28**, 235-242 (2000).
111. L. R. Joyce *et al.*, Streptococcus agalactiae glycolipids promote virulence by thwarting immune cell clearance. *Sci Adv* **10**, eadn7848 (2024).

Figure 1.

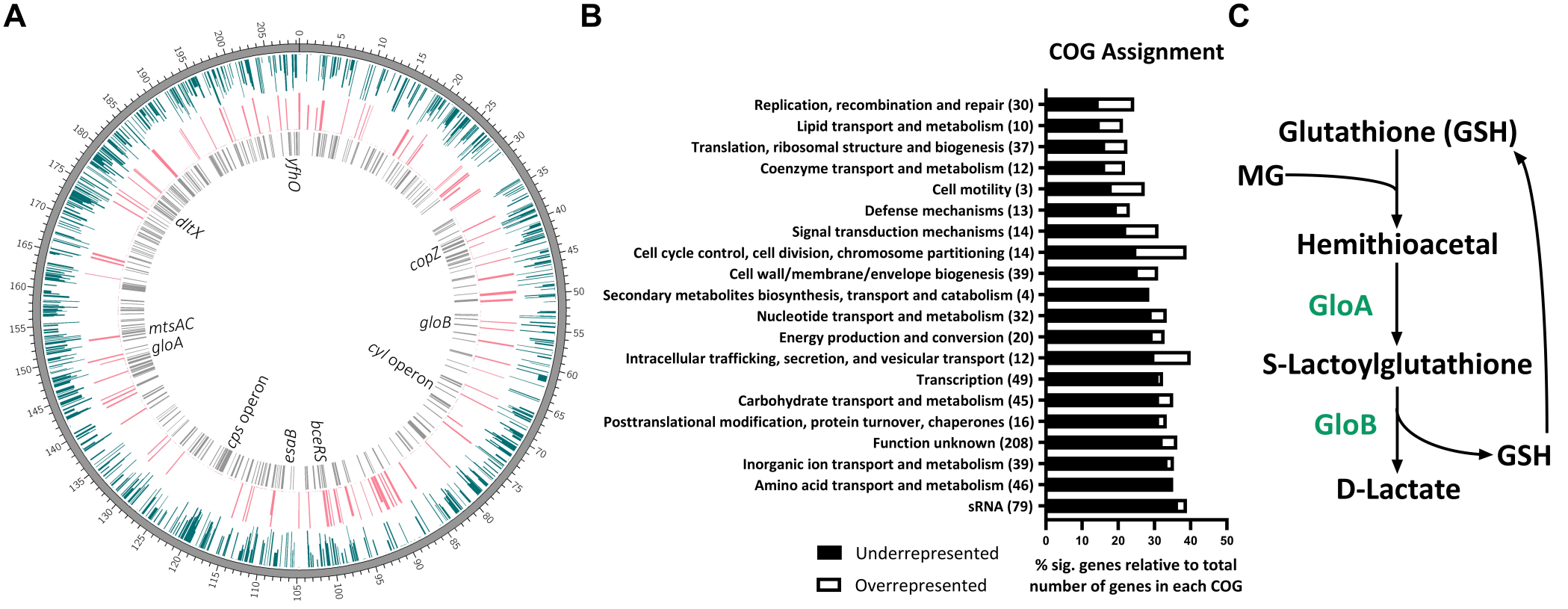
A
yfhO
dltX
copZ
gloB
cyl operon
mtsAC
gloA
cps operon
esaB
bceRS
B
COG Assignment
Replication, recombination and repair (30)
Lipid transport and metabolism (10)
Translation, ribosomal structure and biogenesis (37)
Coenzyme transport and metabolism (12)
Cell motility (3)
Defense mechanisms (13)
Signal transduction mechanisms (14)
Cell cycle control, cell division, chromosome partitioning (14)
Cell wall/membrane/envelope biogenesis (39)
Secondary metabolites biosynthesis, transport and catabolism (4)
Nucleotide transport and metabolism (32)
Energy production and conversion (20)
Intracellular trafficking, secretion, and vesicular transport (12)
Transcription (49)
Carbohydrate transport and metabolism (45)
Posttranslational modification, protein turnover, chaperones (16)
Function unknown (208)
Inorganic ion transport and metabolism (39)
Amino acid transport and metabolism (46)
sRNA (79)
0 10 20 30 40 50
% sig. genes relative to total number of genes in each COG
Underrepresented
Overrepresented
C
Glutathione (GSH)
MG
Hemithioacetal
GloA
S-Lactoylglutathione
GloB
GSH
D-Lactate

Table 1

Locus Tag	Gene Name	Description	Fold Change	Adj. P-value	Function	GBS Reference
Virulence Factors						
ID870_00715	dltX	teichoic acid D-Ala incorporation-associated protein DltX	-21.26	0	Lipoteichoic acid biosynthesis	(*33*)
ID870_01745	scpB	segregation/condensation protein B	-27.67	0	Complement evasion and adhesion	(*34*)
ID870_02600	pil2a-bp	PI-2a subunit	-8.22	0	Adhesion	(*35*)
ID870_04170	esxA1	WXG100 family type VII secretion target	-4.99	0.00432	Type VII Secretion System	(*12*)
ID870_04190	esaB	EsaB/YukD family protein	-20.68	0.02043	Type VII Secretion System	
ID870_05725	iagA	glycosyltransferase	-20.97	0	Lipid biosynthesis	(*36*)
ID870_05905	cylK	CylK protein	-7.11	0.00118	β-hemolysin biosynthesis	(*37, 38*)
ID870_05910	cylJ	CylJ protein	-2.73	0.03089	β-hemolysin biosynthesis	
ID870_05915	cylH/I	beta-ketoacyl-[acyl-carrier-protein] synthase family protein	-4.23	0.0031	β-hemolysin biosynthesis	
ID870_05920	cylF	aminomethyltransferase family protein	-12.91	0	β-hemolysin biosynthesis	
ID870_06030	pil1-bp	PI-1 major pilin	-7.01	0	Adhesion	(*39*)
ID870_07490	brpA	LCP family protein	-4.35	0	Biofilm regulation	(*40*)
ID870_09735	yfhO	YfhO family protein	-9.38	0.00063	Glycan biosynthesis	(*41*)
Capsule						
ID870_02780	capA	CapA family protein	-5.24	0.0017	Capsule biosynthesis	(*22, 42, 43*)
ID870_03485	cps4A	LCP family protein	-6.15	0	Capsule regulation	
ID870_03500	cpsD	tyrosine-protein kinase	-7.36	0	Capsule biosynthesis	
ID870_03505	cpsE	sugar transferase	-9.85	0	Capsule biosynthesis	
ID870_03510	cpsF	UDP-N-acetylglucosamine--LPS N-acetylglucosamine transferase	-26.72	0	Capsule biosynthesis	
ID870_03515	cpsG	multidrug MFS transporter	-28.64	0	Capsule biosynthesis	
ID870_03530	cpsN	glycosyltransferase family 2 protein	-11.31	0	Capsule biosynthesis	
ID870_03535	cpsO	glycosyltransferase family 2 protein	-7.41	0	Capsule biosynthesis	
ID870_03540	cpsJ	glycosyltransferase family 2 protein	-13.36	0	Capsule biosynthesis	
ID870_03545	cpsK	glycosyltransferase family 52 protein	-28.25	0	Capsule biosynthesis	
ID870_03550	cpsL	oligosaccharide flippase family protein	-22.16	0	Capsule biosynthesis	
ID870_03555	neuB	N-acetylneuraminate synthase	-5.21	0	Capsule biosynthesis	
ID870_03560	neuC	UDP-N-acetylglucosamine 2-epimerase (hydrolyzing)	-10.06	0	Capsule biosynthesis	
ID870_03565	neuD	acetyltransferase	-19.97	0	Capsule biosynthesis	
Metal Ion Transport						
ID870_00250	lmb	zinc ABC transporter substrate-binding protein	-7.36	0.01419	Zinc uptake and adhesion	(*44*)
ID870_02010	mtsA	metal ABC transporter substrate-binding protein	-58.89	0	Manganese uptake	(*29*)
ID870_02020	mtsC	metal ABC transporter permease	-7.31	0	Manganese uptake	
ID870_02070	nikA	nickel ABC transporter or nickel/metallophore periplasmic binding protein	-10.85	0	Nickel/copper uptake (putative)	(*29, 45*)

ID870_02660	fhuG	iron ABC transporter permease	-6.41	0	Siderophore-dependent iron uptake	(*46*)
ID870_02665	fhuB	iron ABC transporter permease	-6.50	0	Siderophore-dependent iron uptake	
ID870_05550	mntH	Nramp family divalent metal transporter	-2.87	0.03162	Manganese uptake	(*47*)
ID870_07395	copZ	heavy-metal-associated domain-containing protein	-68.12	0.00559	Copper efflux	(*48*)
ID870_08645	adcC	metal ABC transporter ATP-binding protein	-32.67	0	Zinc uptake	(*44*)
Two-Component Systems (TCS)						
ID870_00330	maeR	response regulator	-6.96	0	Malic acid metabolism regulation (TCS-15)	(*49-51*)
ID870_00705	dltR	response regulator transcription factor	-6.02	0	Lipoteichoic acid regulation (TCS-14)	(*33, 49, 50, 52*)
ID870_04460	ciaH	HAMP domain-containing histidine kinase	-8.63	0	Antimicrobial peptide resistance (TCS-10)	(*49, 50, 53*)
ID870_04495	bceS/nsrK	sensor histidine kinase	-10.41	0.0017	Antimicrobial resistance (TCS-9)	(*49, 50, 54-56*)
ID870_04500	bceR/nsrR	response regulator transcription factor	-20.11	0.00118	Antimicrobial resistance (TCS-9)	
ID870_10420	cssS	HAMP domain-containing histidine kinase	-9.13	0	Two-component system (TCS-19)	(*49, 50*)
Metabolism						
ID870_00585	purA	adenylosuccinate synthase	-15.03	0	Purine metabolism	(*57*)
ID870_02260	**gloA**	lactoylglutathione lyase	-18.38	0	Methylglyoxal detoxification	
ID870_02270	yvgN	aldo/keto reductase	-4.00	0.00518	Aldehyde detoxification	
ID870_02315	glnQ	amino acid ABC transporter ATP-binding protein	-5.28	0.00063	Glutamine transport	(*58*)
ID870_02320	glnP	ABC transporter substrate-binding protein/permease	-4.69	0	Glutamine transport	
ID870_04545	guaA	glutamine-hydrolyzing GMP synthase	-12.55	0	Purine metabolism	(*57, 59*)
ID870_06660	**gloB**	MBL fold metallo-hydrolase	-25.63	0.04532	Methylglyoxal detoxification	
ID870_08815	argH	argininosuccinate lyase	-4.79	0.00063	Arginine metabolism	(*13, 60, 61*)
ID870_09305	purB	adenylosuccinate lyase	-16.22	0	Purine metabolism	(*57*)
ID870_09420	purC	phosphoribosylaminoimidazolesuccinocarboxamide synthase	-27.67	0.00118	Purine metabolism	(*57*)
ID870_09800	guaB	IMP dehydrogenase	-38.05	0	Purine metabolism	(*57, 59*)
ID870_10075	argF	ornithine carbamoyltransferase	-13.36	0	Arginine metabolism	(*13, 60, 61*)
ID870_10080	arcC	carbamate kinase	-9.58	0.00264	Arginine metabolism	

*pvalue < 0.0001 is assigned pvalue of 0 by TRANSIT analysis

Figure 2.

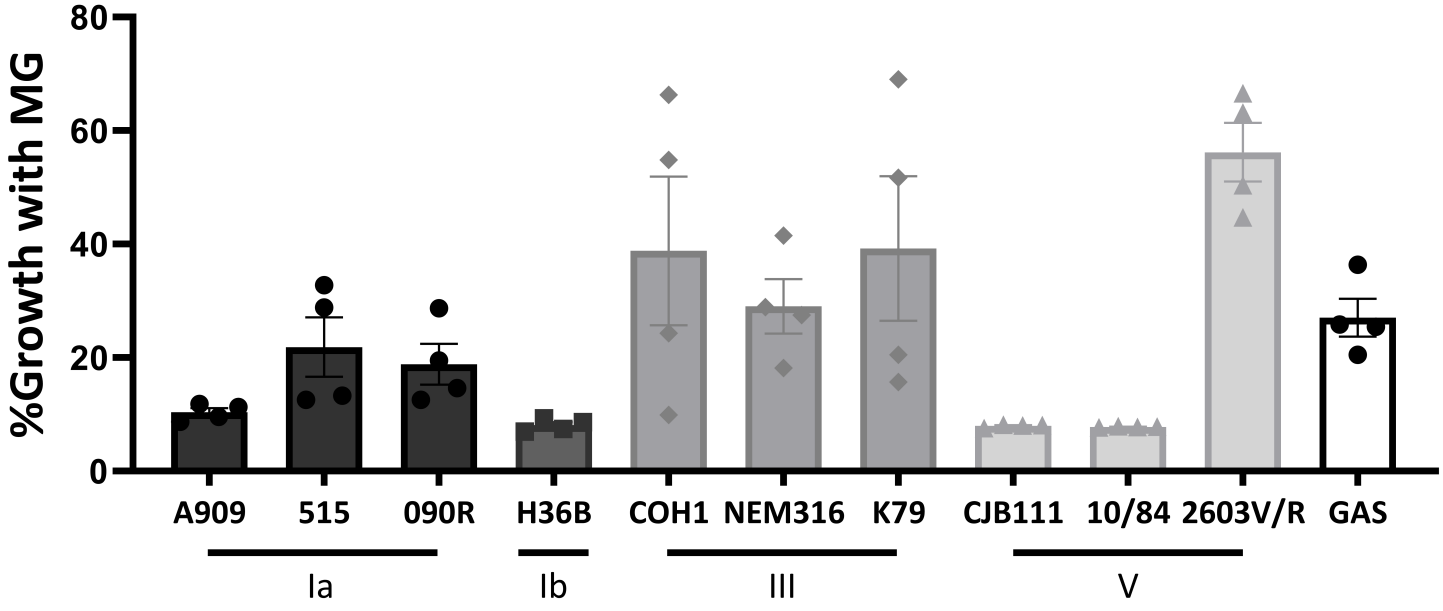
%Growth with MG
80
60
40
20
0
A909
515
090R
H36B
COH1
NEM316
K79
CJB111
10/84
2603V/R
GAS
Ia
Ib
III
V

Figure 3.

A

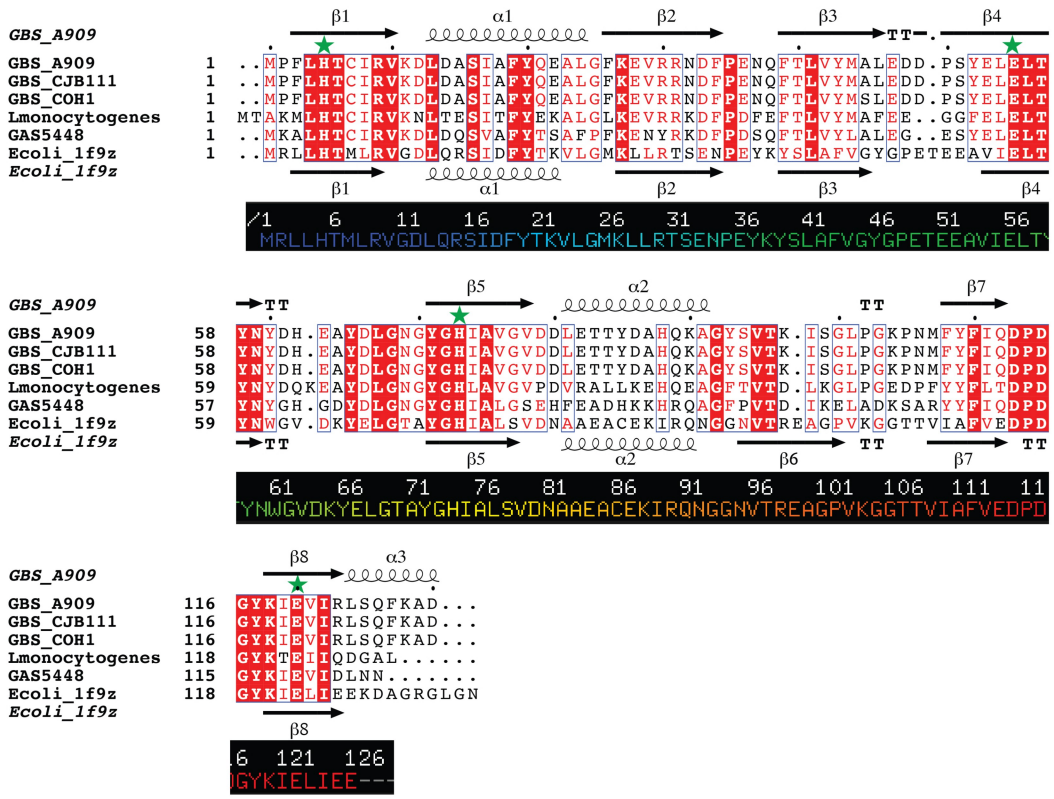

B

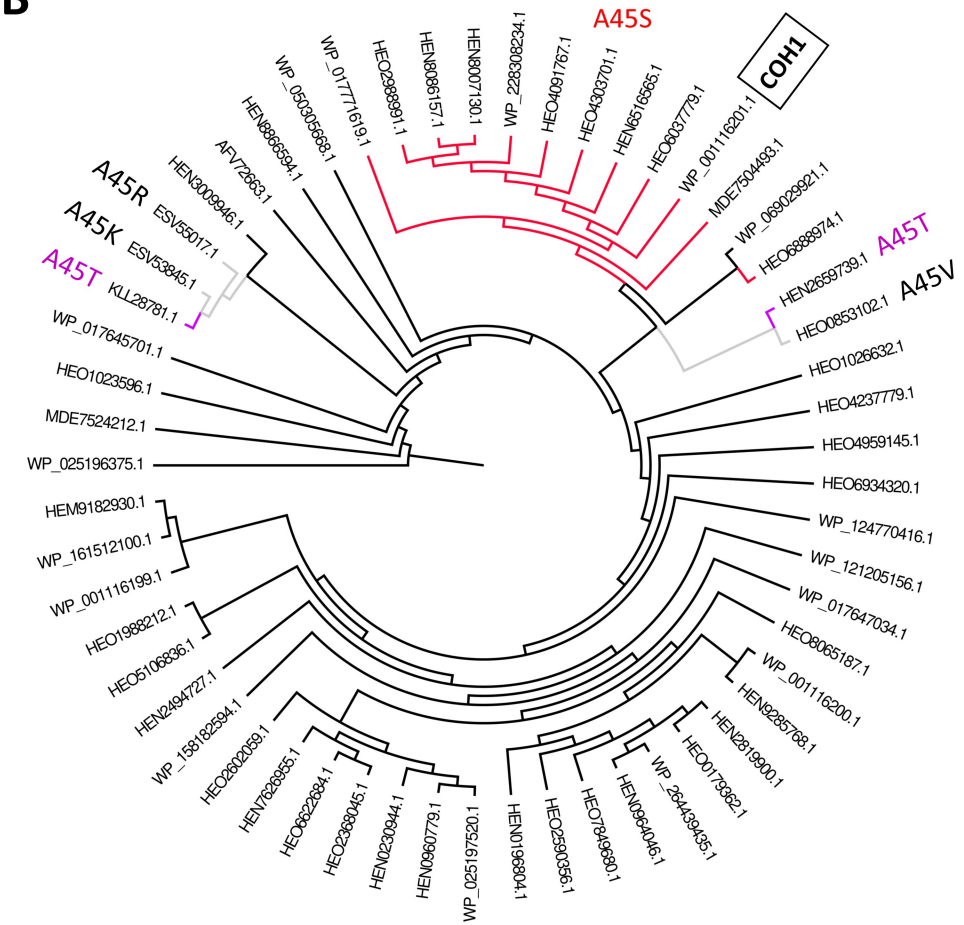

C

E. coli PDB Entry 1F9Z

GBS CJB111/A909 AlphaFold2

E. coli Yellow GBS Cyan

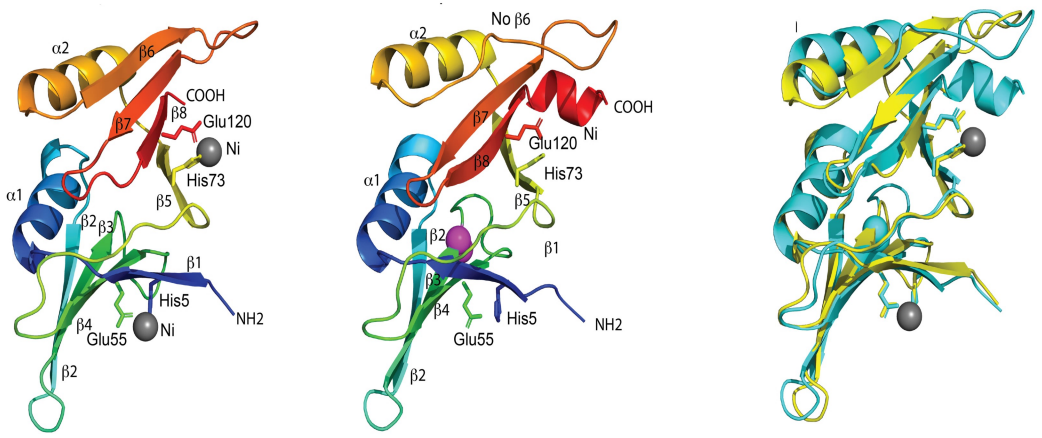

D

GBS CJB111/A909 GloA dimer

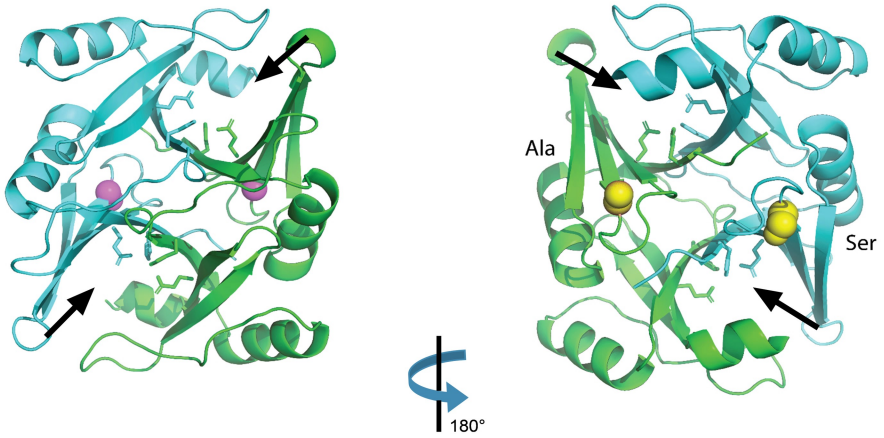

Figure 4.

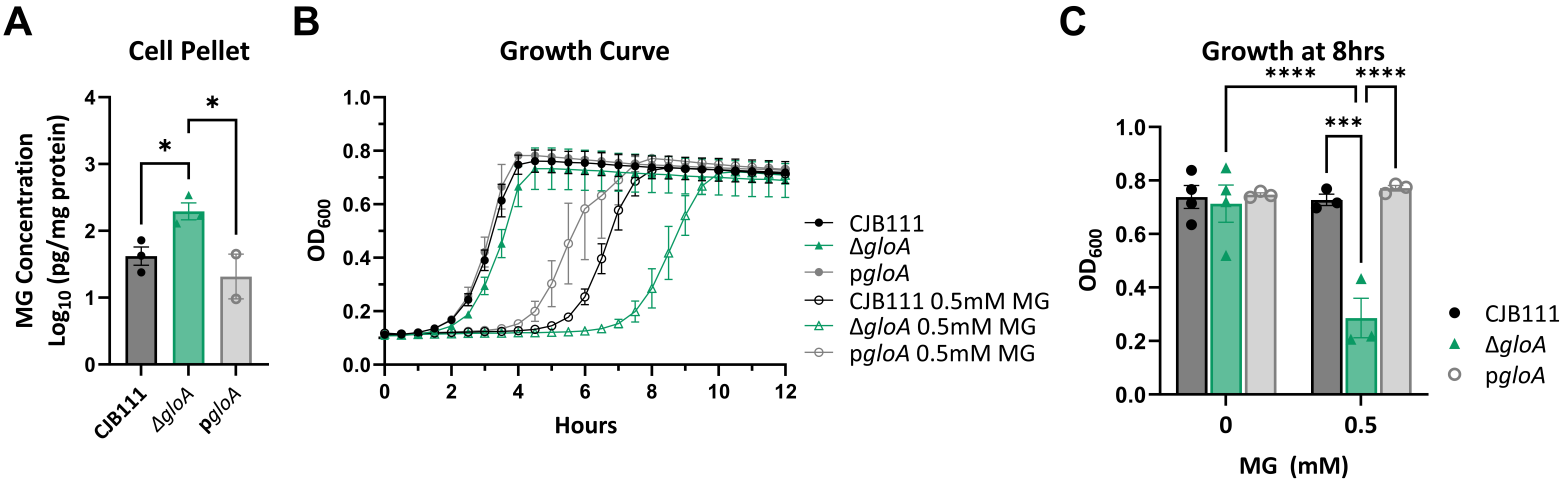
A
Cell Pellet
MG Concentration
Log10 (pg/mg protein)
*
*
CJB111
ΔgloA
pgloA
B
Growth Curve
OD600
Hours
CJB111
ΔgloA
pgloA
CJB111 0.5mM MG
ΔgloA 0.5mM MG
pgloA 0.5mM MG
C
Growth at 8hrs
****
****
***
OD600
MG (mM)
CJB111
ΔgloA
pgloA

Figure 5.

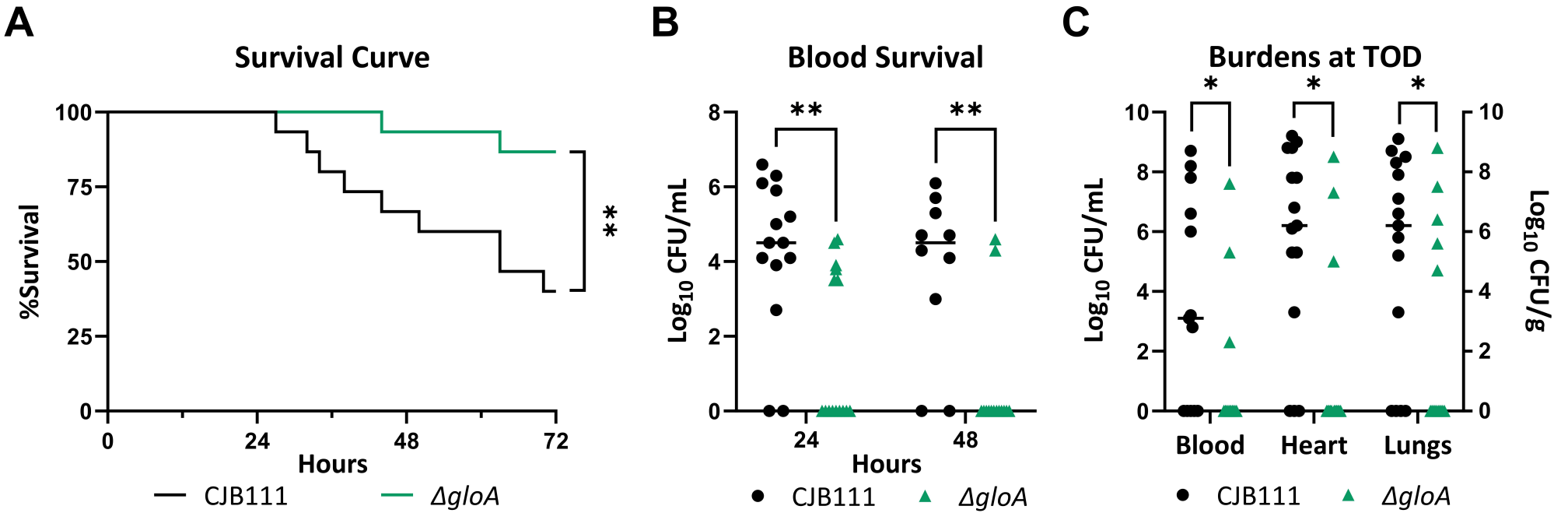
A
Survival Curve
%Survival
100
75
50
25
0
0
24
48
72
Hours
**
CJB111
ΔgloA
B
Blood Survival
Log10 CFU/mL
8
6
4
2
0
**
**
24
48
Hours
CJB111
ΔgloA
C
Burdens at TOD
Log10 CFU/mL
Log10 CFU/g
10
8
6
4
2
0
*
*
*
Blood
Heart
Lungs
CJB111
ΔgloA

Figure 6.

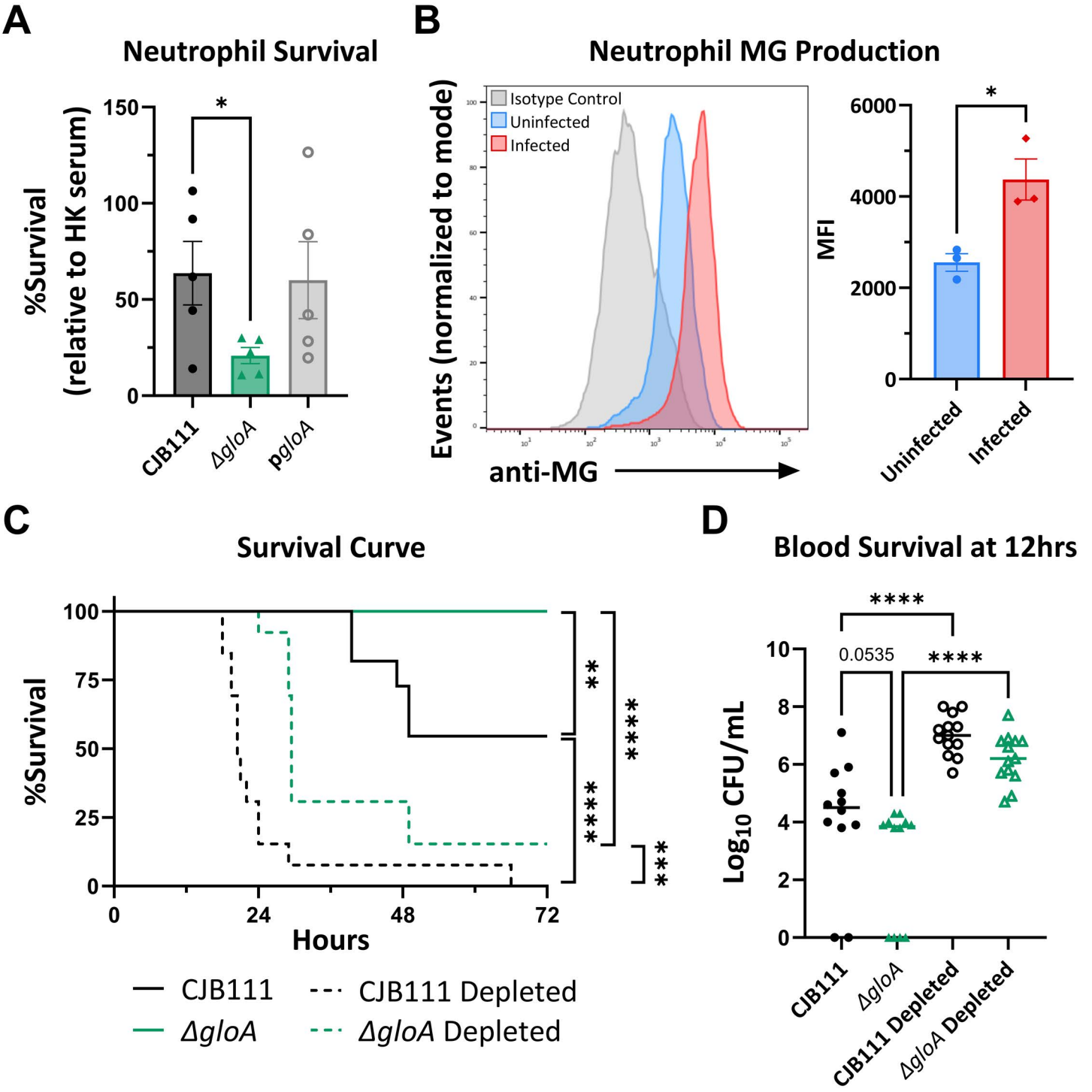
A
Neutrophil Survival
%Survival
(relative to HK serum)
150
100
50
0
*
CJB111
ΔgloA
pgloA
B
Neutrophil MG Production
Isotype Control
Uninfected
Infected
Events (normalized to mode)
anti-MG
6000
4000
2000
0
MFI
*
Uninfected
Infected
C
Survival Curve
%Survival
100
75
50
25
0
0
24
48
72
Hours
**
****
***
**
CJB111
ΔgloA
CJB111 Depleted
ΔgloA Depleted
D
Blood Survival at 12hrs
Log10 CFU/mL
10
8
6
4
2
0
****
0.0535
****
CJB111
ΔgloA
CJB111 Depleted
ΔgloA Depleted